Title
Near-infrared surface plasmon polariton dispersion control with hyperbolic metamaterials

Journal
Optics Express, 21(9)

ISSN
1094-4087

Authors
Luk, Ting S
Kim, Iltai
Campione, Salvatore
et al.

Publication Date
2013-04-29

DOI
10.1364/OE.21.011107

Near-infrared surface plasmon polariton dispersion control with hyperbolic metamaterials

Ting S. Luk,[1,2,*] Iltai Kim,[1,2] Salvatore Campione,[3] Stephen W. Howell,[1] Ganapathi S. Subramania,[1] Robert K. Grubbs,[1] Igal Brener,[1,2] Hou-Tong Chen,[4] Shanhui Fan,[5] and Michael B. Sinclair[1]

[1]*Sandia National Laboratories, 1515 Eubank SE, Albuquerque, NM 87123, USA*
[2]*The Center for Integrated Nanotechnologies, Sandia National Laboratories, Albuquerque, NM 87123, USA*
[3]*Department of Electrical Engineering and Computer Science University of California, Irvine, CA 92697, USA*
[4]*Center for Integrated Nanotechnologies, Los Alamos National Laboratory, Los Alamos, NM 87545, USA*
[5]*Edward L. Ginzton Laboratory, Stanford University, Stanford, California 94305-4088, USA*
[*]*tsluk@sandia.gov*

Abstract: We demonstrate experimentally signatures and dispersion control of surface plasmon polaritons from 1 to 1.8 μm using periodic multilayer metallo-dielectric hyperbolic metamaterials. The fabricated structures are comprised of smooth films with very low metal filling factor. The measured dispersion properties of these hyperbolic metamaterials agree well with calculations using transfer matrix, finite-difference time-domain, and effective medium approximation methods despite using only 2.5 periods. The enhancement factor in the local photonic density of states from the studied samples in the near-infrared wavelength region is determined to be 2.5-3.5. Development of this type of metamaterial is relevant to sub-wavelength imaging, spontaneous emission and thermophotovoltaic applications.

OCIS codes: (240.6680) Surface plasmons; (160.3918) Metamaterials.

References and links

1. A. Boltasseva and H. A. Atwater, "Materials science. Low-loss plasmonic metamaterials," Science **331**(6015), 290–291 (2011).
2. A. Ono, J.-i. Kato, and S. Kawata, "Subwavelength optical imaging through a metallic nanorod array," Phys. Rev. Lett. **95**(26), 267407 (2005).
3. Z. Liu, H. Lee, Y. Xiong, C. Sun, and X. Zhang, "Far-field optical hyperlens magnifying sub-diffraction-limited objects," Science **315**(5819), 1686 (2007).
4. Z. Jacob, L. V. Alekseyev, and E. Narimanov, "Optical hyperlens: far-field imaging beyond the diffraction limit," Opt. Express **14**(18), 8247–8256 (2006).
5. M. Scalora, G. D'Aguanno, N. Mattiucci, M. J. Bloemer, D. de Ceglia, M. Centini, A. Mandatori, C. Sibilia, N. Akozbek, M. G. Cappeddu, M. Fowler, and J. W. Haus, "Negative refraction and sub-wavelength focusing in the visible range using transparent metallo-dielectric stacks," Opt. Express **15**(2), 508–523 (2007).
6. I. I. Smolyaninov, Y.-J. Hung, and C. C. Davis, "Imaging and focusing properties of plasmonic metamaterial devices," Phys. Rev. B **76**(20), 205424 (2007).
7. X. Yang, B. Zeng, C. Wang, and X. Luo, "Breaking the feature sizes down to sub-22 nm by plasmonic interference lithography using dielectric-metal multilayer," Opt. Express **17**(24), 21560–21565 (2009).
8. B. D. F. Casse, W. T. Lu, Y. J. Huang, E. Gultepe, L. Menon, and S. Sridhar, "Super-resolution imaging using a three-dimensional metamaterials nanolens," Appl. Phys. Lett. **96**(2), 023114 (2010).
9. H. N. S. Krishnamoorthy, Z. Jacob, E. Narimanov, I. Kretzschmar, and V. M. Menon, "Topological transitions in metamaterials," Science **336**(6078), 205–209 (2012).
10. X. Yang, J. Yao, J. Rho, X. Yin, and X. Zhang, "Experimental realization of three-dimensional indefinite cavities at the nanoscale with anomalous scaling laws," Nat. Photonics **6**(7), 450–454 (2012).
11. Z. Jacob, J. Y. Kim, G. V. Naik, A. Boltasseva, E. E. Narimanov, and V. M. Shalaev, "Engineering photonic density of states using metamaterials," Appl. Phys. B **100**(1), 215–218 (2010).
12. A. V. Kabashin, P. Evans, S. Pastkovsky, W. Hendren, G. A. Wurtz, R. Atkinson, R. Pollard, V. A. Podolskiy, and A. V. Zayats, "Plasmonic nanorod metamaterials for biosensing," Nat. Mater. **8**(11), 867–871 (2009).

#188139 - $15.00 USD Received 2 Apr 2013; accepted 5 Apr 2013; published 29 Apr 2013

13. I. Kim and K. D. Kihm, "Unveiling Hidden complex cavities formed during nanocrystalline self-assembly," Langmuir **25**(4), 1881–1884 (2009).
14. S. A. Biehs, M. Tschikin, and P. Ben-Abdallah, "Hyperbolic metamaterials as an analog of a blackbody in the near field," Phys. Rev. Lett. **109**(10), 104301 (2012).
15. C. Otey and S. Fan, "Numerically exact calculation of electromagnetic heat transfer between a dielectric sphere and plate," Phys. Rev. B **84**(24), 245431 (2011).
16. R. S. Ottens, V. Quetschke, S. Wise, A. A. Alemi, R. Lundock, G. Mueller, D. H. Reitze, D. B. Tanner, and B. F. Whiting, "Near-field radiative heat transfer between macroscopic planar surfaces," Phys. Rev. Lett. **107**(1), 014301 (2011).
17. E. Rousseau, A. Siria, G. Jourdan, S. Volz, F. Comin, J. Chevrier, and J.-J. Greffet, "Radiative heat transfer at the nanoscale," Nat. Photonics **3**(9), 514–517 (2009).
18. P. J. van Zwol, L. Ranno, and J. Chevrier, "Tuning near field radiative heat flux through surface excitations with a metal insulator transition," Phys. Rev. Lett. **108**(23), 234301 (2012).
19. S. Shen, A. Narayanaswamy, and G. Chen, "Surface phonon polaritons mediated energy transfer between nanoscale gaps," Nano Lett. **9**(8), 2909–2913 (2009).
20. M. De Zoysa, T. Asano, K. Mochizuki, A. Oskooi, T. Inoue, and S. Noda, "Conversion of broadband to narrowband thermal emission through energy recycling," Nat. Photonics **6**(8), 535–539 (2012).
21. M. Francoeur, R. Vaillon, and M. P. Menguc, "Thermal impacts on the performance of nanoscale-gap thermophotovoltaic power generators," IEEE Trans. Energy Conv. **26**(2), 686–698 (2011).
22. A. V. Shchegrov, K. Joulain, R. Carminati, and J. J. Greffet, "Near-field spectral effects due to electromagnetic surface excitations," Phys. Rev. Lett. **85**(7), 1548–1551 (2000).
23. S. Basu, Z. M. Zhang, and C. J. Fu, "Review of near-field thermal radiation and its application to energy conversion," Int. J. Energy Res. **33**(13), 1203–1232 (2009).
24. O. Ilic, M. Jablan, J. D. Joannopoulos, I. Celanovic, and M. Soljacić, "Overcoming the black body limit in plasmonic and graphene near-field thermophotovoltaic systems," Opt. Express **20**(S3), A366–A384 (2012).
25. M. Laroche, R. Carminati, and J. J. Greffet, "Near-field thermophotovoltaic energy conversion," J. Appl. Phys. **100**(6), 063704 (2006).
26. A. Narayanaswamy and G. Chen, "Surface modes for near field thermophotovoltaics," Appl. Phys. Lett. **82**(20), 3544–3546 (2003).
27. G. V. Naik, J. Liu, A. V. Kildishev, V. M. Shalaev, and A. Boltasseva, "Demonstration of Al:ZnO as a plasmonic component for near-infrared metamaterials," Proc. Natl. Acad. Sci. U.S.A. **109**(23), 8834–8838 (2012).
28. G. V. Naik, J. L. Schroeder, X. Ni, A. V. Kildishev, T. D. Sands, and A. Boltasseva, "Titanium nitride as a plasmonic material for visible and near-infrared wavelengths," Opt. Mater. Express **2**(4), 478–489 (2012).
29. J. B. Pendry, L. Martín-Moreno, and F. J. Garcia-Vidal, "Mimicking surface plasmons with structured surfaces," Science **305**(5685), 847–848 (2004).
30. F. J. Garcia-Vidal, L. Martin-Moreno, and J. B. Pendry, "Surfaces with holes in them: new plasmonic metamaterials," J. Opt. A, Pure Appl. Opt. **7**(2), S97–S101 (2005).
31. N. F. Yu, Q. J. Wang, M. A. Kats, J. A. Fan, S. P. Khanna, L. H. Li, A. G. Davies, E. H. Linfield, and F. Capasso, "Designer spoof surface plasmon structures collimate terahertz laser beams," Nat. Mater. **9**(9), 730–735 (2010).
32. C. R. Williams, S. R. Andrews, S. A. Maier, A. I. Fernandez-Dominguez, L. Martin Moreno, and F. J. Garcia-Vidal, "Highly confined guiding of terahertz surface plasmon polaritons on structured metal surfaces," Nat. Photonics **2**(3), 175–179 (2008).
33. A. P. Hibbins, B. R. Evans, and J. R. Sambles, "Experimental verification of designer surface plasmons," Science **308**(5722), 670–672 (2005).
34. M. L. Nesterov, D. Martin-Cano, A. I. Fernandez-Dominguez, E. Moreno, L. Martin-Moreno, and F. J. Garcia-Vidal, "Geometrically induced modification of surface plasmons in the optical and telecom regimes," Opt. Lett. **35**(3), 423–425 (2010).
35. J. T. Shen, P. B. Catrysse, and S. H. Fan, "Mechanism for designing metallic metamaterials with a high index of refraction," Phys. Rev. Lett. **94**(19), 197401 (2005).
36. S. Q. Li, P. J. Guo, L. X. Zhang, W. Zhou, T. W. Odom, T. Seideman, J. B. Ketterson, and R. P. H. Chang, "Infrared plasmonics with indium-tin-oxide nanorod arrays," ACS Nano **5**(11), 9161–9170 (2011).
37. C. L. Cortes, W. Newman, S. Molesky, and Z. Jacob, "Quantum nanophotonics using hyperbolic metamaterials," J. Opt. **14**(6), 063001 (2012).
38. Z. Shi, G. Piredda, A. C. Liapis, M. A. Nelson, L. Novotny, and R. W. Boyd, "Surface plasmon polaritons on metal-dielectric nanocomposite films," in OSA Technical Digest (CD) (Optical Society of America, 2009), IThG6.
39. S. Tomita, T. Yokoyama, H. Yanagi, B. Wood, J. B. Pendry, M. Fujii, and S. Hayashi, "Resonant photon tunneling via surface plasmon polaritons through one-dimensional metal-dielectric metamaterials," Opt. Express **16**(13), 9942–9950 (2008).
40. I. Avrutsky, I. Salakhutdinov, J. Elser, and V. Podolskiy, "Highly confined optical modes in nanoscale metal-dielectric multilayers," Phys. Rev. B **75**(24), 241402 (2007).
41. Y. Yagil, P. Gadenne, C. Julien, and G. Deutscher, "Optical properties of thin semicontinuous gold films over a wavelength range of 2.5 to 500 μm," Phys. Rev. B **46**(4), 2503–2511 (1992).

#188139 - $15.00 USD Received 2 Apr 2013; accepted 5 Apr 2013; published 29 Apr 2013

42. M. Hövel, B. Gompf, and M. Dressel, "Dielectric properties of ultrathin metal films around the percolation threshold," Phys. Rev. B **81**(3), 035402 (2010).
43. B. Gompf, J. Beister, T. Brandt, J. Pflaum, and M. Dressel, "Nanometer-thick Au-films as antireflection coating for infrared light," Opt. Lett. **32**(11), 1578–1580 (2007).
44. J. Schilling, "Uniaxial metallo-dielectric metamaterials with scalar positive permeability," Phys. Rev. E Stat. Nonlin. Soft Matter Phys. **74**(4), 046618 (2006).
45. W. Cai and V. Shalaev, *Optical Metamaterials Fundamentals and applications* (Springer, 2010).
46. S. V. Zhirnov and D. I. Sementsov, "Surface polaritons in a thin layer of an anisotropic superconductor," Opt. Spectrosc. **104**(3), 467–474 (2008).
47. C. H. Gan and P. Lalanne, "Well-confined surface plasmon polaritons for sensing applications in the near-infrared," Opt. Lett. **35**(4), 610–612 (2010).
48. K.-P. Chen, V. P. Drachev, J. D. Borneman, A. V. Kildishev, and V. M. Shalaev, "Drude relaxation rate in grained gold nanoantennas," Nano Lett. **10**(3), 916–922 (2010).
49. W. Chen, K. P. Chen, M. D. Thoreson, A. V. Kildishev, and V. M. Shalaev, "Ultrathin, ultrasmooth, and low-loss silver films via wetting and annealing," Appl. Phys. Lett. **97**(21), 211107 (2010).

In recent years, there has been a growing interest in the use of local photonic density of states (LPDOS) enhancement of surface plasmon polariton (SPP) states in the near-infrared (NIR) [1] region (0.8-3 μm) for a vast range of applications including sub-wavelength imaging [2–8], spontaneous emission enhancement [9–11], nanobiosensing [12, 13], near-field energy transfer enhancement [14–19], and near-field thermophotovoltaics [20–26]. Therefore, the ability to control LPDOS through the SPP dispersion remains at the forefront of research. While encouraging progress has been made in the development of low-loss NIR plasmonic materials [27, 28], metamaterials can potentially offer a viable solution to the lack of low-loss plasmonic materials at NIR wavelengths.

The use of an array of cut-off waveguides to effectively reduce the plasma frequency of a metal from its bulk value, and thereby control the SPP dispersion was first proposed by Pendry et al. [29, 30], and subsequently verified experimentally at microwave frequencies [12, 31–33]. Since then, many metamaterial designs have been proposed to control SPP dispersion in the NIR range [34–36]. However, most of the proposed schemes (e.g., metal gratings and nanowire arrays) require high aspect ratios and/or submicron structural features, which are rather difficult to fabricate. To alleviate this difficulty, here we employ a design which consists of simple periodic multilayer metallo-dielectric structures to produce the metal-dilution effect. In the wavelength region and metal filling factors investigated here, the structure is referred to as a type II hyperbolic metamaterial [37], which possesses a uniaxial anisotropic dielectric tensor, with metal-like properties in the direction parallel to the surface (i.e. $\varepsilon_{\parallel} < 0$), and dielectric-like properties in the direction perpendicular to the surface (i.e. $\varepsilon_{\perp} > 0$). This type of structure has been used to create ultrahigh optical index cavities for broadband radiative emission control [10]. In this work, we focus on using the surface modes of hyperbolic metamaterials to create a concentrated narrow band electromagnetic energy through LPDOS control. Although the existence of SPP [38, 39] and bulk plasmon modes [40] of hyperbolic material have been previously shown, we here fully characterize the dispersion properties and demonstrate tunability as well as the validity of using effective medium approximations for Au-SiO_2 multilayer metallo-dielectric hyperbolic metamaterials. The measured characteristics are in good agreement with calculations using the transfer matrix method (TMM), finite-difference time-domain (FDTD) approaches, and the effective medium approximation (EMA). This design offers flexibility and controllability of the SPP dispersion of the mode located at the air-metal interface.

The samples investigated in this work are composed of alternating layers of Ti-Au (1 nm of Ti as an adhesion layer and 5 nm of Au) and SiO_2 (50, 100 or 250 nm) [see Fig. 1(a)], called sample A, B and C, respectively. The thin films were sequentially deposited on a glass substrate using thermal evaporation with a base vacuum pressure of 10^{-7} torr. A total of 5 layers (i.e., 2.5 periods) were deposited, with the top layer being Au. The dielectric functions of the constituent materials (Ti-Au, SiO_2, and glass substrate) were independently determined

#188139 - $15.00 USD Received 2 Apr 2013; accepted 5 Apr 2013; published 29 Apr 2013

by ellipsometry measurements over the spectral range between 0.3 and 5 μm (VVASE and IRVASE from J.A. Woollam). The results reveal that the Ti layer does not introduce any noticeable change to the fitted dielectric function of the Ti-Au bilayer and therefore the bilayer is treated as a single layer in our calculations. The measured Au dielectric function shows Drude-like behavior with a negative real part of the permittivity which monotonically decreases with wavelength. The dielectric function also exhibits a monotonic increase in AC conductivity with wavelength, a clear signature that the film is above the percolation threshold [41, 42]. The reported percolation threshold thickness for Au is 6.5nm with no adhesion layer [42, 43]. The presence of Ti adhesion layer is expected to reduce the percolation thickness to a smaller value. A cross-sectional SEM image of sample B is shown in Fig. 1(b), and topographic images of the Ti, Ti-Au and SiO_2 films obtained using atomic force microscopy are shown in Fig. 1(c)-1(e). The high quality of the films demonstrated by these images enables us to control the short wavelength limit of the SPP dispersion of Au from 1.0 μm to 1.8 μm, as we will show later.

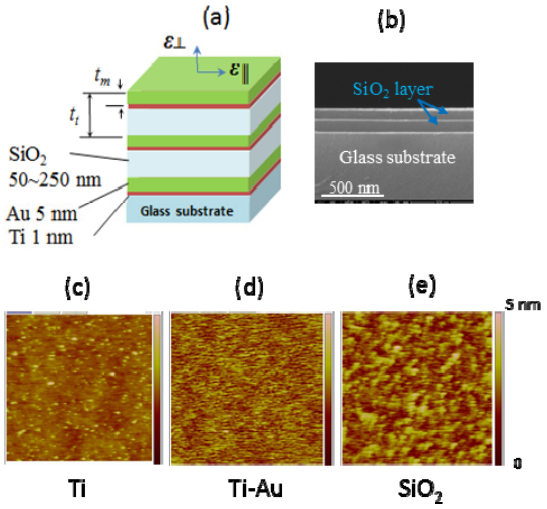

Fig. 1. (a) Schematic depiction of 2.5 periods of metallo-dielectric hyperbolic metamaterial composed of alternating layers of Ti-Au (1 nm thick Ti and 5 nm thick Au), and SiO_2 (50, 100 or 250 nm); sample A, B and C respectively. Thin films are sequentially deposited on a glass substrate using thermal evaporation with a base vacuum pressure of 10^{-7} torr. (b) Cross-sectional SEM image shows clear identification of 3 layers of Au and 2 layers of SiO_2 films (100 nm thick). (c-e) AFM topography images of 1 nm thick Ti, 5nm thick Au on 1 nm thick Ti, and 100nm thick SiO_2 film for a 1.0μm × 1.0μm region in the peak-to-valley grey scale of 0-5 nm range with their respective root mean square roughness of 0.2, 0.4 and 0.4 nm.

The classic signature for the identification of the SPP mode is the presence of a reflectivity minimum at the SPP resonance frequency for *p*-polarized light using prism coupled attenuated total internal reflection (ATR) measurements. Conventionally, the ratio R_p/R_s is measured to reduce systematic errors, where R_p and R_s are reflectivities of *p*- and *s*-polarized light, respectively. These measurements were performed using an ATR apparatus mounted on the previously mentioned ellipsometers for accurate angle and polarization control. The results of ATR and non-ATR (i.e., with the prism removed) R_p/R_s measurements for sample B are shown in Fig. 2(a) and 2(b), respectively. The ATR measured R_p/R_s exhibits a prominent minimum [Fig. 2(a)] which is absent in the non-ATR ratio [Fig. 2(b), a signature of a SPP resonance excitation. As an additional confirmation, we obtained the absorption spectrum from the transmission and reflection measurements without prism coupling (data not shown) and did not observe any absorption feature that corresponds to the reflectivity

#188139 - $15.00 USD Received 2 Apr 2013; accepted 5 Apr 2013; published 29 Apr 2013

minimum at the SPP resonance wavelength from the ATR measurements, as expected from a SPP state.

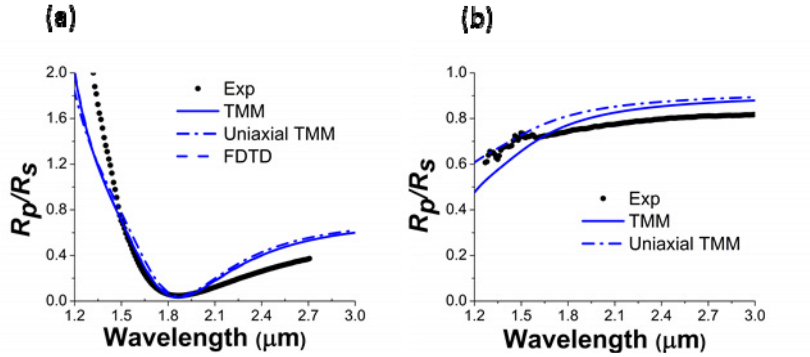

Fig. 2. The classic signatures for the identification of SPP mode of sample B at 45 degree angle of incidence. (a) The presence of a reflectivity minimum at the SPP resonance using ATR configuration. (b) Its absence without ATR. Experiments are depicted as black circular symbols. Results obtained from 5-layer TMM, single layer of uniaxial effective medium TMM, and FDTD calculations are solid (blue online), dash-dot (blue online), and dash (blue online) lines, respectively. Due to the close match of FDTD result with TMM calculation, they cannot be distinguished visually.

Figure 3(a) shows the experimentally measured SPP dispersion curve which was obtained by measuring the wavelength of the ATR minimum as a function of the angle of incidence. We simulated the dispersion curve using the TMM method as follows: Using the previously measured dielectric function for the Ti/Au bilayer as a starting point, we used the TMM method for the 5-layer stack to fit the R_p/R_s reflectivity curve at a single angle (usually 45 deg.) to obtain a slightly modified dielectric function for the metal layer in the full stack. In this fitting procedure all layer thickness were held at their as-designed values. The fitted curve is shown in Fig. 2(a). The fit obtained shows good agreement in the region of minimum reflectivity with slight deviation away from the minimum location. This difference is caused by inaccuracy of the Au dielectric function, and non-uniformities in thicknesses and dielectric properties of the film stack. Next, keeping all thicknesses and dielectric functions constant, we used the TMM method to generate R_p / R_s for different angles of incidence, thereby mapping out the SPP dispersion curve shown in Fig. 3(a).

We also utilized the effective medium description of the metamaterial to simulate the behavior of the multilayer samples. As noted previously, the effective properties of the multilayer metallo-dielectric metamaterial can be described by a uniaxial hyperbolic material whose dispersion relation [44] is given by, $\frac{k_\perp^2}{\varepsilon_\parallel}+\frac{k_\parallel^2}{\varepsilon_\perp}=k_0^2$ where the subscripts "||" and "$\perp$" indicate the directions parallel (in-plane) and perpendicular (out-of-plane) to the surface, respectively (notice the notation here for parallel and perpendicular are reverse of Schilling's notation [44]), and k and k_0 are the wavevectors in the medium and vacuum, respectively. The uniaxial anisotropic dielectric functions can be evaluated using mean field approach [45]: $\varepsilon_\parallel = f\,\varepsilon_m + (1-f)\varepsilon_d$ and $1/\varepsilon_\perp = f/\varepsilon_m + (1-f)/\varepsilon_d$, where ε_m and ε_d are the dielectric functions of the metal and dielectric layers, respectively, and $f = t_m/t_t$ is the metal filling factor, with t_m and t_t being the thicknesses of metal and metamaterial period, respectively, as depicted in Fig. 1(a). For a small filling factor, the real part of $\varepsilon_\perp$ is almost the same as the real part of ε_d, whereas its imaginary part becomes significantly larger than the imaginary part of ε_d due to the contribution from the lossy metal. On the other hand, both the real and

#188139 - $15.00 USD Received 2 Apr 2013; accepted 5 Apr 2013; published 29 Apr 2013

imaginary part of $\varepsilon_{\parallel}$ are reduced greatly by about a factor of f when compared to ε_m. Therefore, varying the metal filling factor of the metamaterial structure offers a promising and effective way to control the SPP frequency. The trade-off of this control is a reduction of the most commonly used figure of merit (FOM) defined as the ratio of real and imaginary parts of the dielectric function. The FOM for the new effective medium plasmonic material can be related to the FOM of its metal constituent by, $\frac{|\varepsilon'_{//}|}{\varepsilon''_{//}} = \frac{|\varepsilon'_m|/\varepsilon''_m - (1-f)\varepsilon'_d/(f\varepsilon''_m)}{1+(1-f)\varepsilon''_d/(f\varepsilon''_m)}$ where the single and double primes represent the real and imaginary parts of the dielectric functions. From this expression, we can easily see that the FOM of the effective medium is always smaller than its metal constituent. For the samples A, B and C, their peak FOMs values are reduced by a factor of 1.6, 1.8 and 2.3, respectively.

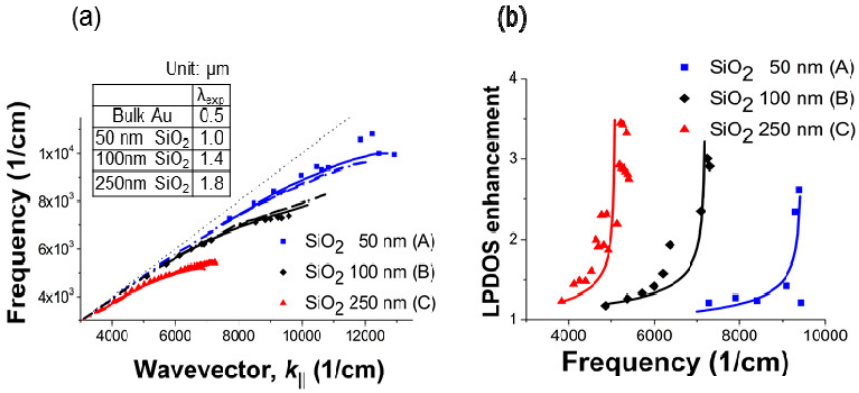

Fig. 3. (a) Surface plasmon dispersion curves from three different metal filling factor samples (A, B and C) of 0.118, 0.076 and 0.032 arising from a different SiO_2 thickness: 50 nm in blue, 100 nm in black, and 250 nm in red, respectively. Experimental data from sample A, B and C are indicated by symbols of squares (blue online), diamonds (black online), and triangles (red online). Dispersion calculations using 5-layer TMM, single layer of uniaxial effective medium, and analytical solution are solid, dash, and dash-dot lines, respectively. Notice the dispersion results of uniaxial TMM and analytical solution are in quite good agreement. The free space light line is indicated by a light dotted line. The inset table summarizes the experimentally obtained shortest SPP wavelengths for the three samples. (b) LPDOS enhancement of the three samples mentioned above. The solid lines are for the purpose of visual guide.

To explicitly show the hyperbolic nature of the material, we treat the film stack as a single layer of uniaxial effective medium material, and calculate R_p/R_s using the TMM. This will be referred to as the single layer uniaxial TMM model from here on. The ATR reflectivity of sample B obtained from the single layer uniaxial TMM model is shown in Fig. 2(a). The dielectric functions $\varepsilon_{\parallel}$ and $\varepsilon_{\perp}$ of the layer are obtained from the equations provided above. For small metal filling factors, $\varepsilon_{\perp}$ remains largely unchanged from its dielectric constituent, whereas $\varepsilon_{\parallel}$ will depend sensitively on the metal filling factor. Since our samples (A, B & C) all have only 2.5 periods with three layers of metal and two layers of dielectric, the metal filling factor is expected to be 50% higher than the value of an infinite medium which is given by the ratio of the metal thickness to the period. We determine the effective metal filling factor and the effective thickness of the film stack by fitting the R_p/R_s reflectivity curve for a single angle of incidence using uniaxial TMM model. The obtained metal filling factors for sample A, B and C are 0.118, 0.076 and 0.032 which are 31%, 58% and 63% higher than their corresponding infinite medium values of 0.09, 0.048, and 0.0196, respectively. The $\varepsilon_{\parallel}$ dielectric functions obtained from this procedure are shown in Fig. 4.

#188139 - $15.00 USD Received 2 Apr 2013; accepted 5 Apr 2013; published 29 Apr 2013

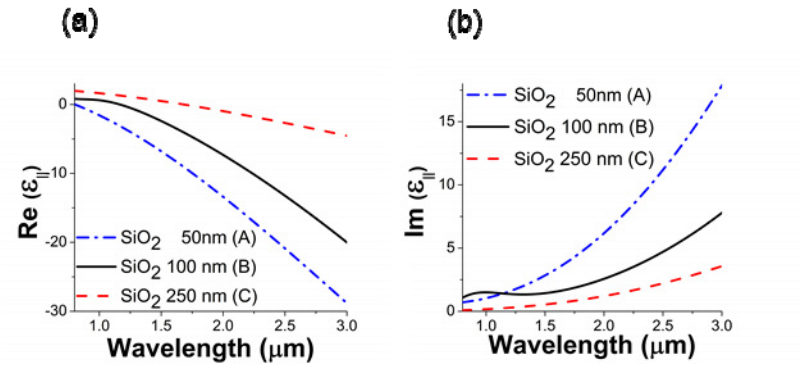

Fig. 4. The real (a) and imaginary (b) parts of $\varepsilon_{\parallel}$ of the uniaxial anisotropic dielectric functions of sample A, B, and C obtained from fitted ellisopmetry data. The sample A, B, and C with metal filling factor f = 0.118, 0.076, and 0.032, respectively are depicted by a dash-dot (blue online), solid, and dash (red online) lines, respectively. In part a, sample A, B, and C becomes a type II hyperbolic metamaterial at wavelengths beyond 0.8, 1.2, and 1.7 μm, respectively since $\varepsilon_{\parallel}$ is negative, whereas $\varepsilon_{\perp}$ is positive in the entire wavelength range for all samples (data not shown).

Once the filling fraction and the dielectric functions have been determined, the SPP dispersion curves for the uniaxial effective medium are obtained by varying the angle of incidence in the TMM simulations. In addition, the SPP dispersion curves for a single layer of uniaxial effective medium material of finite thickness t_t can be obtained analytically from the transcendental equation [46]

$$\left(\frac{\varepsilon_1}{\sqrt{k_{\parallel}^2-\varepsilon_1 k_0^2}}+\frac{\varepsilon_{\parallel}}{\alpha}\right)\left(\frac{\varepsilon_{\parallel}}{\alpha}+\frac{\varepsilon_{sub}}{\sqrt{k_{\parallel}^2-\varepsilon_{sub}k_0^2}}\right)+\left(\frac{\varepsilon_1}{\sqrt{k_{\parallel}^2-\varepsilon_1 k_0^2}}-\frac{\varepsilon_{\parallel}}{\alpha}\right)\left(\frac{\varepsilon_{\parallel}}{\alpha}-\frac{\varepsilon_{sub}}{\sqrt{k_{\parallel}^2-\varepsilon_{sub}k_0^2}}\right)\exp(-2\alpha t_t)$$

where α is $\sqrt{\varepsilon_{\parallel}(\varepsilon_{\perp}^{-1}k_{\parallel}^2-k_0^2)}$, ε_{sub} is the dielectric function of glass substrate, and $\varepsilon_1=1$ for SPP located at the air-sample interface. The analytical SPP dispersion obtained by solving the transcendental equation using an iterative numerical method shows good agreement with that obtained from the uniaxial TMM calculations as shown in Fig. 3(a). It is worth noting that the dispersion equation based on semi-infinite uniaxial material [47] can only provide qualitative agreement (data not shown).

Since LPDOS control depends on the ability to tune the dispersion of SPP, we fabricated two other samples with 50 and 250 nm thick SiO_2 layers (sample A and C) to demonstrate this design flexibility. The experimentally determined dispersion curves of these samples are also shown in Fig. 3(a). We obtained similarly good agreement with the measured SPP dispersion using the 5-layer TMM, the single layer uniaxial TMM model, and the analytical calculations as sample B. The values of the short wavelength limit of the SPP, near the maximum wavevector, are shown in the inset table of Fig. 3(a). From these samples, we demonstrated experimentally more than 3x increase in the SPP wavelength compared to bulk Au by changing the metal filling factor. The LPDOS can be estimated from the measured dispersion curves of the structure by observing that the LPDOS is proportional to $dk/d\omega = 1/v_g$, where v_g is the group velocity. The LPDOS enhancement factors with respect to free space determined from the experimental data for the three fabricated samples are plotted in Fig. 3(b). The maximum LPDOS values observed from the three samples are in the range of

#188139 - $15.00 USD Received 2 Apr 2013; accepted 5 Apr 2013; published 29 Apr 2013

2.5-3.5, where these values are limited by the angular steps and spectral resolution of the experimental data taken. We expect significantly higher enhancement factor can be realized using low-loss Ag as metal.

The identification of these resonances as SPPs is also supported by FDTD simulations using a commercially available package (Lumerical Inc.) which show the expected electric field pattern [shown in Fig. 5(a)] and enhanced electric field intensity near the surface (shown in Fig. 5(b)) for a SPP state. The reflectivity ratio on the top metal surface retrieved from the FDTD simulation results is in very good agreement with 5-layer TMM calculations (shown in Fig. 2(a)). The square of the field is enhanced by a factor 14 when the incidence angle is 45°, and the 1/e intensity decay length normalized to the SPP wavelength is 0.2 [47]. For additional confirmation that the 5-layer stack can be treated as effective medium, we performed FDTD simulation on a single uniaxial layer of effective medium using the in-plane and out-of-plane dielectric functions obtained from ellipsometry, and using a thickness equal to that of the entire multilayer. The surface normal component of the electric field pattern of the SPP mode [shown in Fig. 5(c)] obtained closely resembles that of the multilayer.

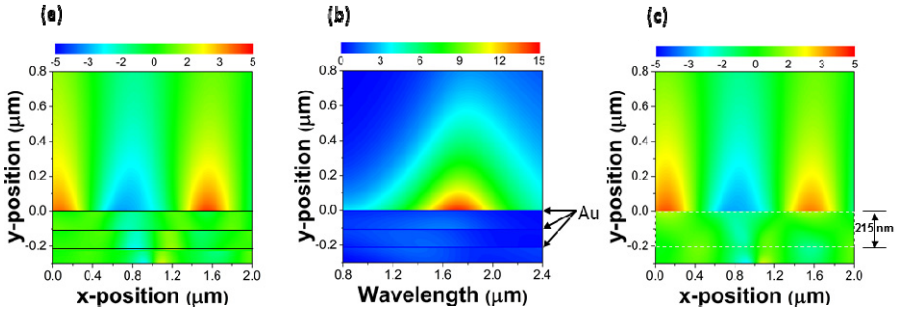

Fig. 5. The result of a FDTD simulation of the field pattern and enhancement signatures of the SPP resonance for sample B. The top air-metal interface is at y-position = 0 and the bottom metal-substrate interface is at y-position = –0.215μm. The metal layers are indicated with black lines. A *p*-polarized incident field is launched from the bottom inside the glass substrate to the film stack at an angle of incidence of 45 degrees. (a) The surface normal component of the electric field pattern of the SPP located on the top air-metal interface. (b) The wavelength dependent enhancement factor for the electric field amplitude square normalized to the incident value. (c) The electric field mode pattern same as (a) for a single layer of a uniaxial effective medium with thickness equal to that of the entire 5-layer stack.

In summary, we have experimentally demonstrated SPP dispersion control using high quality hyperbolic metamaterials consisting of Au-SiO_2 metallo-dielectric multilayer thin films with metal filling factors ranging from 0.032 to 0.118. We have found that the experimentally observed SPP dispersion can be accurately described using 5-layer TMM, the uniaxial TMM model, FDTD, and EMA calculations. The hyperbolic nature of the material is also explicitly demonstrated. In addition, we observed a 2.5-3.5 fold enhancement in the local photonic density of state for the frequency range and filling factors explored in this paper. We expect the photonic density of state enhancement can be significantly improved with the use of Ag or by annealing the samples [48, 49].

Acknowledgments

The authors acknowledge stimulating discussions with Yong Zeng, and Young Chul Jun. This work was performed, in part, at the Center for Integrated Nanotechnologies, an Office of Science User Facility operated for the U.S. Department of Energy (DOE) Office of Science and Office of Basic Energy Science. Sandia National Laboratories is a multi-program laboratory managed and operated by Sandia Corporation, a wholly owned subsidiary of Lockheed Martin Corporation, for the U.S. Department of Energy's National Nuclear Security Administration under contract DE-AC04-94AL85000.